TITLE PAGE

Citation Format:

Marco Renna, Mauro Buttafava, Anurag Behera, Marta Zanoletti, Laura Di Sieno, Alberto Dalla Mora, Davide Contini, and Alberto Tosi, " Multi-wavelength dual-detection channel system for time-resolved near-infrared spectroscopy," in Optical Tomography and Spectroscopy of Tissue XIII, S. Fantini, P. Taroni ed., Vol 10874 of Proceedings of SPIE (SPIE, Bellingham, WA, 2019), paper 1087408.

Copyright notice:

DOI abstract link:

https://doi.org/10.1117/12.2509706

Multi-wavelength dual-detection channel system for time-resolved near-infrared spectroscopy

Marco Renna, Mauro Buttafava, Anurag Behera, Marta Zanoletti, Laura Di Sieno, et al.

Marco Renna, Mauro Buttafava, Anurag Behera, Marta Zanoletti, Laura Di Sieno, Alberto Dalla Mora, Davide Contini, Alberto Tosi, "Multi-wavelength dual-detection channel system for time-resolved near-infrared spectroscopy," Proc. SPIE 10874, Optical Tomography and Spectroscopy of Tissue XIII, 1087408 (1 March 2019); doi: 10.1117/12.2509706

SPIE.

Event: SPIE BiOS, 2019, San Francisco, California, United States

Multi-wavelength, dual-detection channel system for time-resolved near-infrared spectroscopy

Marco Renna[a], Mauro Buttafava[a], Anurag Behera[b], Marta Zanoletti[b], Laura Di Sieno[b], Alberto Dalla Mora[b], Davide Contini[b], Alberto Tosi*[a]

[a]Dipartimento di Elettronica, Informazione e Bioingegneria, Politecnico di Milano, Milan, Italy
[b]Dipartimento di Fisica, Politecnico di Milano, Milan, Italy
*alberto.tosi@polimi.it

ABSTRACT

We present a new full-custom instrument for time-domain diffuse optical spectroscopy developed within Horizon 2020 LUCA (Laser and Ultrasound Co-Analyzer for thyroid nodules) project. It features eight different picosecond diode lasers (in the 635 – 1050 nm range), two 1.3 x 1.3 mm^2 active-area SiPMs (Silicon PhotoMultipliers) working in single-photon mode and two 10 ps resolution time-to-digital converters. A custom FPGA-based control board manages the instrument and communicates with an external computer via USB connection. The instrument proved state-of-the-art performance: an instrument response function narrower than 160 ps (fullwidth at half-maximum), a long-term measurement stability better than 1%, and an output average optical power higher than 1 mW at 40 MHz. The instrument has been validated with phantom measurements.

Keywords: Diffuse optics, near-infrared spectroscopy, pulsed laser, single-photon detector, time-resolved, time-correlated single-photon counting, time-to-digital converter;

1. INTRODUCTION

Thanks to the recent advancements of photonic technologies, measurement techniques based on weak light signals are now widespread among many research fields such as medicine, biochemistry, automotive, quantum cryptography and many more [1]-[3]. The possibility to investigate faint and fast phenomena down to the picosecond time-scale is fostering the diffusion of photonic instrumentation in many laboratories all over the world. An example is the Near-InfraRed Spectroscopy (NIRS) which takes advantage of the theories developed within the Diffuse Optics (DO) [4] to non-invasively probe biologic tissues or pharmaceutical products by means of monochromatic light at different wavelengths [2],[5],[6]. Instruments based on Continuous Wave (CW) illumination and detection are widely diffused and wearable devices based on CW technology are currently under development [7]. Despite low-cost and low system complexity, CW instrument lack of accuracy in retrieving absolute constituent concentrations in layered tissues, especially when a single source-detector pair is used. Moreover, they are sensitive to movements and variation of shallow layers of the sample, leading to low repeatability of the measurements [8]-[10]. On the other hand, systems based on a Time-Resolved (TR) approach allow to overcome these limitations, as the capability to acquire the Distribution of Time-Of-Flight (DTOF) curves permits to add a further dimension to the measurement, allowing to clearly distinguish between absorption and scattering effects [11] and breaking the trade-off between source-detector distance and penetration depth [10],[12],[13]. TR approach thus allows to reduce the source-detector distance with respect to CW techniques, leading to a higher Signal-to-Noise Ratio (SNR) [14]. The main drawback of TR instrument is a high system complexity besides high-costs, due to the use of picosecond pulsed laser sources, single-photon detectors and time-measurement units with picosecond timing resolution and high-linearity performance [7].

In this work we developed a state-of-the-art time-resolved NIRS instrument featuring eight different wavelengths in the near-infrared range and two detection channels with singe-photon counting capability, still guaranteeing compact dimensions and a 5x cost reduction with respect to multi-wavelength instrument based on commercial photonic components. Two detection-channels also allow to implement a double-distance measurement scheme (one light injection point and two detection points placed at two different distances), improving accuracy in estimating constituents

Optical Tomography and Spectroscopy of Tissue XIII, edited by Sergio Fantini, Paola Taroni, Proc. of SPIE
Vol. 10874, 1087408 · © 2019 SPIE · CCC code: 1605-7422/19/$18 · doi: 10.1117/12.2509706

in multi-layer tissues. Moreover, a wide range of output wavelengths permits to better discriminate among various sample constituents, providing more information on the sample.

2. SYSTEM DESIGN

The presented instrument (its simplified block diagram is shown in Fig. *1*) consists of all the fundamental parts of a TCSPC instrument for Time-Resolved NIRS (TR NIRS), as it includes: i) eight custom picosecond pulsed laser sources based on commercially-available laser diodes, emitting in the near-infrared range (600-1100 nm); ii) two custom wide-area (1.3 x 1.3 mm^2) detector modules based on commercially available Silicon Photomultipliers (SiPMs) used in single-photon regime; iii) two high-precision time-measurement units whose core is a custom Time-to-Digital Converter (TDC) ASIC with around 40 ps (Full Width at Half-Maximum –FWHM) single-shot precision [15]; iv) a custom control board based on an FPGA, which reconstructs the measurement DTOF curves and transfers data to the external computer.

Optical pulses emitted by the laser sources are coupled into eight independent 100 µm-core fibers. Each fiber is connected to an in-fiber adjustable attenuator, each one tuned to the specific laser wavelength providing an attenuation up to 40 dB. The output of each attenuator is connected to a 9 x 1 optical switch, used to select the instrument output wavelength. The ninth channel of the switch is left unconnected in order to provide no laser output when no measurement is running, in compliance with safety regulation for a clinical environment. Laser pulses at the switch output are injected into the sample through a 100 µm-core fiber and the backscattered light is collected by means of two 1 mm-core glass optical fibers in order to maximize light harvesting. The output of each fiber is coupled to the active-area of the respective SiPM-based detector through a custom optical system.

The FPGA manages the instrument, since it: i) provides the trigger signals to the laser sources; ii) reads data from the two TDCs and reconstructs the measurement histograms of the photon arrival-times; iii) controls the 9x1 optical switch and the eight independent adjustable attenuators; iv) transfers data to a remote computer through a controller USB 2.0. A graphical user interface allows to tailor the measurement parameters to the specific application, thus fostering the possibility to adopt this instrument in various application besides TR NIRS, where sub-nanosecond laser sources and single-photon detectors are required.

The instrument is housed in a standard 19" industrial rack case (dimensions are 48 x 38 x 20 cm^3) and provides at its output 8 General Purpose Input/Outputs (GPIOs) and four wide-bandwidth connections, thus allowing to integrate the instrument in more complex measurement setups. The instrument is powered starting either from a 230 V AC (50 Hz) or 110 V AC (60 Hz) rails, which is converted to 24 V DC thanks to a medical grade AC/DC converter. A dedicated custom power board is used to distribute the power supply to all the instrument sub-components.

In the following sections we provide a detailed description of the complete instrument.

2.1 Compact, multiwavelength pulsed laser module

Laser sources suitable for a TR NIRS instrument should guarantee: i) light emission at multiple wavelength in the

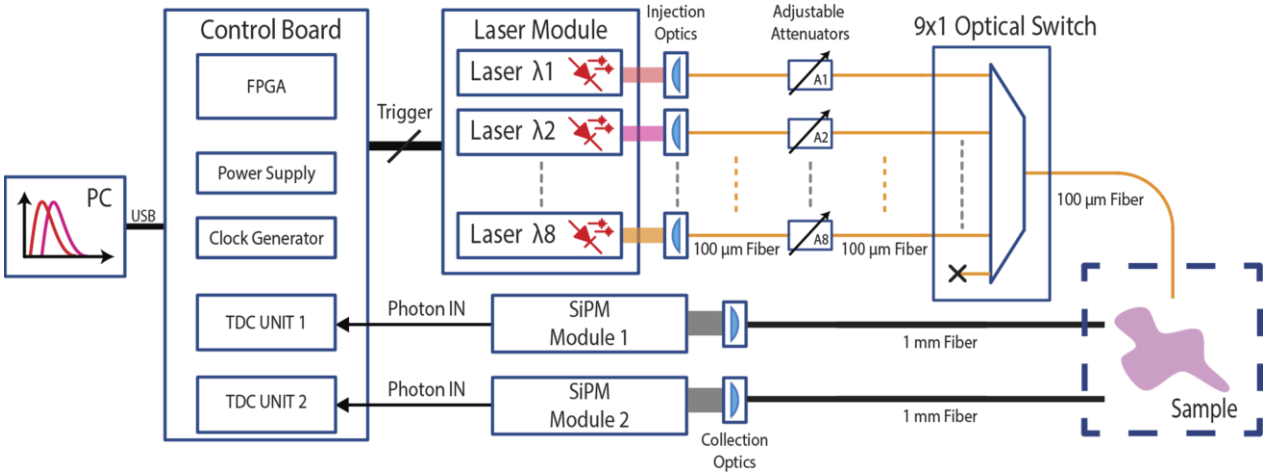

Fig. 1 Simplified block diagram of the instrument.

near-infrared region; ii) pulse energy generally higher than 25 pJ (i.e. 1 mW average optical power at 40 MHz pulse repetition rate); iii) pulse repetition rate equal or higher than 40 MHz; iv) optical pulse width narrower than 200 ps [16] (FWHM); v) temporal and thermal stability better than ±1% of both optical power and shape of the optical pulses.

Laser sources based on edge-emitting laser diodes are now a standard choice when high pulse repetition rate and compact dimensions are required, with small compromise on energy of the optical pulses. Commercially-available pulsed diode lasers offer performance matching the design requirements in terms of optical power, pulse repetition rate and temporal duration of the optical pulses (see [17],[18] and others) but, on the other hand, manufacturers generally do not offer customization in terms of dimensions and high costs generally prevent the design of compact multiwavelength systems based on multiple commercial laser sources.

In order to overcome such limitations, we designed a compact fully-custom multiwavelength pulsed laser module featuring eight independent diode lasers based on commercially-available edge-emitting laser diodes. The selected wavelengths and optical performance are reported in Table I, with wavelength ranging from 635 to 1050 nm, pulse width narrower than 135 ps (FWHM) and average free-space optical power in the mW range at 40 MHz repetition rate. The core of the module is the laser diode pulser board, which is a revised version of the laser pulser described in [19], operating laser diodes in Gain-Switching regime [20] at a repetition rate adjustable up to 120 MHz. The current pulse temporal duration can be adjusted, through a pulse-shaper circuit, between 0.5 and 5 ns. Laser diodes are placed on one edge of the laser diode pulser board and housed in a standard collimation package (from Thorlabs Inc.). We chose laser diodes in standard TO package as a reference for our design due to the large availability of wavelengths and the possibility to use standard optics and housing components. The eight laser diode pulsers are all mounted on a host Printed Circuit Board (PCB) which provides eight independent, user-adjustable power supplies for the laser diode pulser. A microcontroller on the host board guarantees a safe turn on/off procedure, stores the operating parameters of the laser diode pulsers and communicates with the instrument control board.

Optimal temporal and thermal stability performance over few hours of operation are achieved thanks to two custom-made thermal systems:

- A heating circuit, utterly described in [21], is mounted on each laser diode pulser and guarantees constant temperature of the driving circuitry (55°C), thus avoiding any temporal shift nor shape variation of the current pulse that drives the laser diode. Heating was preferred to cooling to reduce power dissipation and system complexity.
- A cooling system based on a Thermo-Electric Cooler (TEC) and a custom mechanical mounting system. Laser heads are kept at 16°C and are coupled two-by-two in the mechanical assembly to reduce the overall dimensions and number of components. A custom TEC driver PCB, mounted below the laser pulser host board, hosts the four independent TEC drivers and is controlled by the instrument control board via I^2C bus.

The output of each laser source is coupled in a 100 μm-core optical fiber through a commercially-available optical system with pitch-yaw adjustment. The eight fiber-injection systems and the laser module PCB assembly are mounted on a rectified aluminum board for mechanical stability. Optical couplings ranging from 40% to 80% are obtained,

Table I. Optical performance of the presented instrument.

Wavelength [nm]	**Fiber-coupled average power [a] [mW]**	**Optical coupling**	**Pulse-width [b] [ps]**	**Warm-up time [c] [min]**
635	3.3	70%	105	25
670	4.7	54%	135	35
730	1.1	76%	75	50
830	4.1	79%	110	50
852	2.6	42%	115	15
915	3.4	69%	100	25
980	3.1	74%	95	30
1050	3.5	49%	115	15

[a]Measured at 40 MHz pulse repetition rate.
[b]Temporal duration of the optical pulse, Full Width at Half-Maximum.
[c]For 3 hours ±1% measurement stability.

depending on the selected laser source. The complete pulsed laser module has dimensions of 26 x 26 x 8 cm^3, a maximum power consumption lower than 30 W and provides state-of-the-art performance, with a cost reduction of about a factor five with respect to systems based on commercial laser sources based on edge-emitting laser diodes.

2.2 SiPM-Based Single-Photon Detectors

Photodetectors for TR NIRS systems should have timing jitter lower than 100 ps (FWHM), sufficient Photo-Detection Efficiency (PDE) and a wide active-area (1 mm^2 or more) in order to maximize the light harvesting [16]. Single-photon detectors based on PhotoMultiplier Tubes (PMTs) and Micro-Channel Plates (MCPs) can offer optimum performance in terms of both dimensions of the active-area and PDE [22], but they generally lack of robustness (can be damaged due to strong illumination), which is a fundamental parameter for an instrument designed for a clinical environment. Single-Photon Avalanche Diodes (SPADs) in single-photon counting mode offer robustness besides optimal timing performance with a timing jitter lower than 30 ps (FWHM), a PDE higher than 60% at 500 nm and still 12% at 800 nm [23],[24]. Unfortunately, SPADs have small active-area (in the order of 0.01 mm^2 or slightly higher), thus they do not fit design specifications for a TR NIRS instrument. SiPMs technology has faced an exponential growth in the last few years, with timing performance approaching SPAD ones, but providing active-areas which can be few orders of magnitude wider. Detectors based on SiPMs demonstrated single-photon sensitivity with timing jitter of about 100 ps (FWHM) with Dark Count Rate (DCR) lower than 100 kcps for devices cooled slightly below room temperature [25].

For the presented instrument we designed an upgraded version of the SiPM-based detector described in [26], and two identical replicas are equipped, one for each detection channel. With respect to the previous design, we adopted a 1.3 x 1.3 mm^2 active-area SiPM (Hamamatsu Photonics KK) and a two-stage amplification circuit based on a Monolithic Microwave Integrated Circuit (MMIC). These two improvements led to timing jitter of 70 ps (FWHM) with PDE equal to 38% at 500 nm and 8% at 800 nm. The detector is housed in a standard TO package and cooled down to 10°C with a two-stage TEC, needed to keep the DCR lower than 50 kcps. Each detector is housed in a compact aluminum case (dimensions are 50 x 40 x 110 mm^3), is powered starting from a single 15 V DC rail and exhibits a maximum power consumption of 8 W (at the maximum count rate of 150 Mcps).

2.3 System Control Board and Time-Measurement Electronics

Linearity and jitter performance of the time-measurement instrumentation play a major role in a TCSPC acquisition system, as any distortion of the DTOF curves may affect the post-processing fitting algorithm. TCSPC systems with excellent linearity performance (<1% LSB) are commercially available, featuring picosecond timing resolution and single-shot precision lower than 10 ps (FWHM) [27], [28], but they are too bulky and expensive for a multichannel TCSPC system, thus preventing a wide diffusion of TR NIRS instrumentation in clinical and biomedical fields.

In this project, we developed two custom time-measurement units, mounted on the control board, as shown in Fig. *2*. An Artix 7 FPGA (Xilinx Inc.) reads the TDC units data and runs the instrument measurement routine. Every time a single conversion is complete, the FPGA, reads the photon arrival-time data and builds up the DTOF curves which are provided to the external computer through an USB 2.0 link once the measurement is complete, i.e. at the end of the measurement integration time (user-adjustable between 0.3 and 16 s per each wavelength). Real-time data acquisition is obtained thanks to a memory swapping algorithm, as described in [19], which allows to download data while a new measurement is running. The eight laser trigger signals are provided by the FPGA starting from a programmable crystal-based oscillator, whose output frequency is user-adjustable between 1 and 100 MHz at 1 MHz steps. The standard instrument repetition frequency is set at 40 MHz. To improve system flexibility an external synchronization source can be used, which is read through a low-jitter comparator. When the internal clock source is used, a copy of the signal is provided on one of the auxiliary wide-bandwidth outputs, allowing to integrate the instrument in more complex setups.

The two time-measurement units are based on a custom TDC ASIC fabricated in standard 0.35 μm HV CMOS technology [15] and provide a timing resolution equal to 10 ps, with a single-shot precision of about 40 ps (FWHM), 80 ns Full-Scale Range (FSR) and a DNL equal to 0.9% LSB. Voltage pulses at detector output are read with negligible jitter through a wide-bandwidth front-end comparator with user-adjustable threshold and each TDC units measures the photon arrival times in a reverse start-stop approach: the TDC START signal is provided by the "Photon IN" signal and the STOP by the measurement synchronization signal (i.e. a copy of the laser trigger signal), thus maximizing the instrument conversion rate.

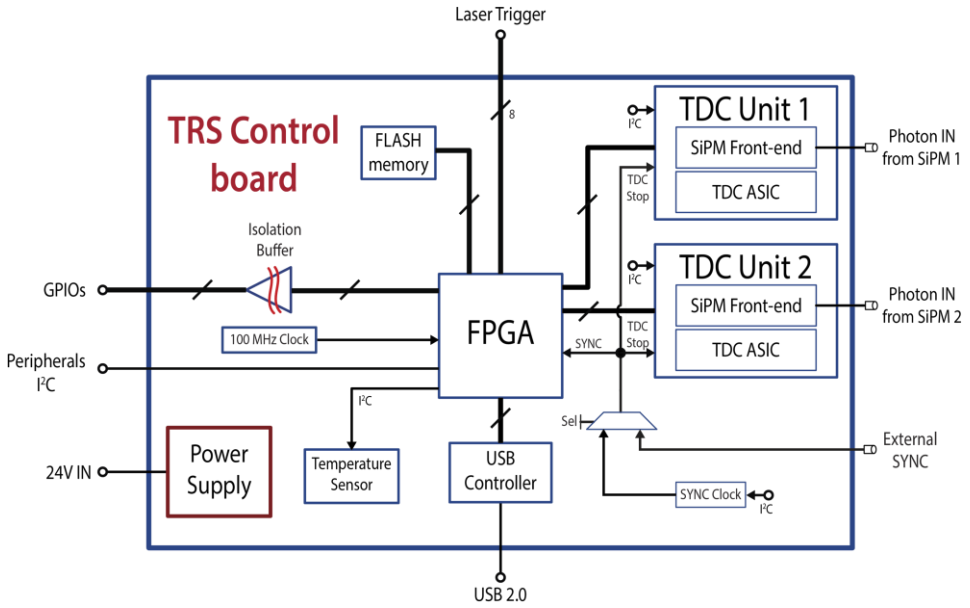

Fig. 2 Simplified block diagram of the instrument control board. Data from the two time-measurement units are acquired by the FPGA, which reconstructs the TCSPC histograms and transfers them to the PC via USB 2.0. A FLASH memory stores the firmware of the FPGA, whose time-base is set by a high stability 100 MHz clock source. The FPGA communicates with the instrument peripherals through an I^2C Bus and provides 8 General Purpose Input/Outputs (GPIOs) for external customizable signals, with electrical isolation of the FPGA guaranteed by an isolation buffer.

3. EXPERIMENTAL CHARACTERIZATION

The complete instrument is shown in Fig. 3 and its performance were assessed through a deep experimental characterization. Measurement results are provided in the following sections.

3.1 Instrument Response Function and TCSPC validation

The Instrument Response Function (IRF) for the 830 nm laser source is shown in Fig. 5-a, with a temporal duration equal to 145 ps (FWHM), which includes the optical pulse width, the detector timing jitter and the single-shot precision of the

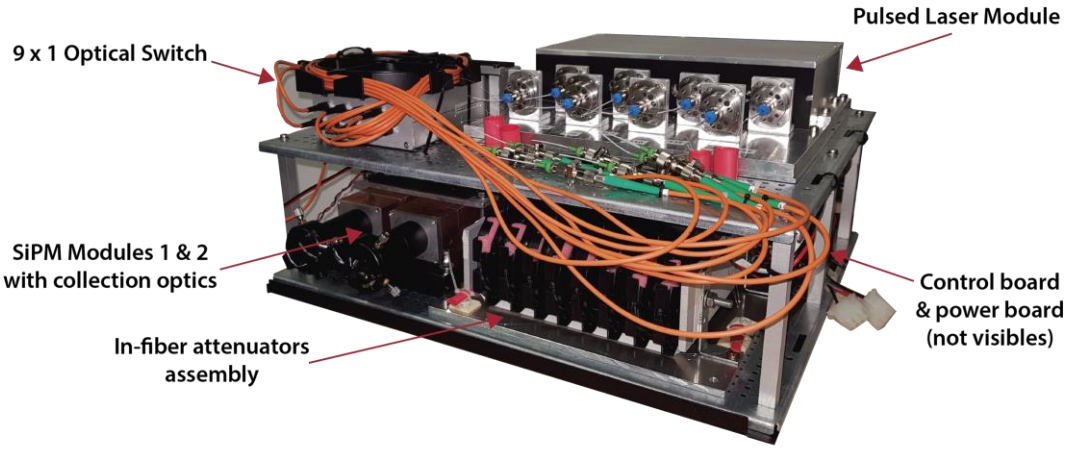

Fig. 3 Picture of the developed instrument mounted in the industrial 19" case. On the top floor are placed the pulsed laser module with fiber injection optics (right) and the 9 x 1 optical switch (left). Below the pulsed laser module are placed the eight in-fiber adjustable attenuators. SiPM-based photodetectors are placed below the optical switch in order to maximize the distance between the avalanche signal pick-up circuitry and the laser diode pulsers, thus avoiding ElectroMagnetic Interference (EMI). On the rear of the attenuator assembly is placed the dedicated power board (not visible) and the control board is placed beneath the separator of the two floors.

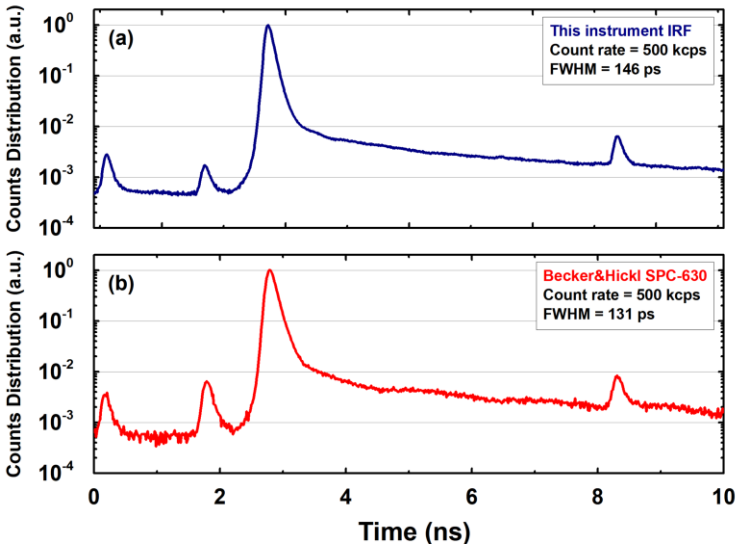

Fig. 5 (a) Normalized Instrument Response Function using the 830 nm laser source and (b) DTOF curve obtained using a B&H SPC-630 acquisition board. The same laser source and single-photon detector were used. The measurement results exhibit a good matching between the two acquisition systems.

time-measurement unit. The IRF was acquired at 40 MHz measurement repetition rate, with a detection count rate equal to 500 kcps, thus guaranteeing distortion due to pile-up effects well below 1%. Measurement was performed directly coupling the 100 µm-core output optical fiber of the 9 x 1 optical switch and the 1 mm-core collection fiber of the SiPM 2 photodetector, connected to TDC unit 2. The multiple reflections at fiber junctions visible in the IRF do not affect the measurement since the region-of-interest of the reconstructed optical pulses for spectroscopic measurement extends only few nanoseconds after the main peak.

To further validate the TCSPC acquisition channel, we split the detector output and provided it to a Becker & Hickl SPC-630 acquisition board. Measurement synchronization signal was provided through one of the auxiliary wide-bandwidth connection of the instrument. The acquired DTOF curve is shown in Fig. 5-b and correctly matches the

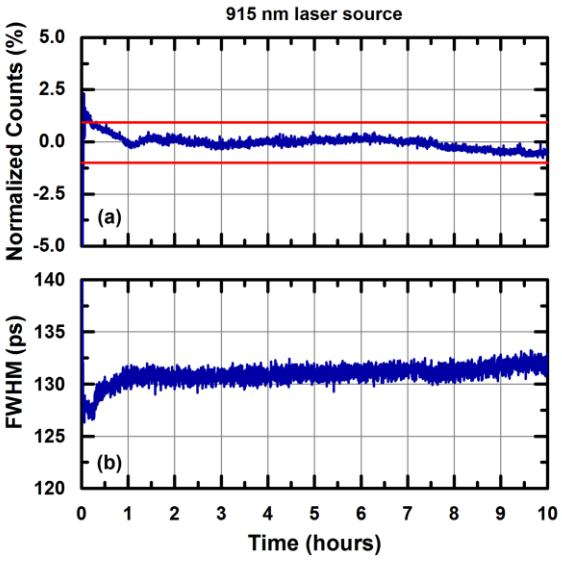

Fig. 4 Stability over time of the IRF for the 915 nm laser source. (a) Normalized count-rate variation, which reflects potential drifts of either the laser source output power or the detection efficiency of the SiPM-based detector. Variations remain below ±1% after about 25 minutes warm-up time. (b) Temporal width of the IRF, which exhibits a variation of few picoseconds over 10 hours of measurement, after warm-up.

IRF acquired with the presented instrument.

3.2 Stability performance

In order to validate the optical stability performance of the instrument, we acquired the IRF for all the eight laser sources from system turn-on for several hours of operation. Measurement was performed as reported in sect. 3.1 and IRFs were acquired with round-robin fashion, with 2 seconds integration time per each wavelength, at 40 MHz repetition rate. Fig. 4 shows the measurement results for the 915 nm laser source, where SiPM 2 and TDC Unit 2 were used. As highlighted by the two horizontal red lines, which mark the ±1% range around the count-rate mean value, after less than 30 minutes from turn-on, stability is reached and maintained over 10 hours of operation with negligible fluctuations, allowing to perform long-time measurements without the need to acquire the IRF multiple times during a measurement session.

3.3 Validation on solid phantoms

To validate the capability of the instrument to correctly retrieve absorption and reduced scattering coefficient of a sample, we performed a validation on solid phantoms [29] made of titanium dioxide particle (scattering agent) and toner powder (absorbing agent), embedded in an epoxy resin matrix, and a sub-set of the obtained results is shown in Fig. 6. We present two set of measurements:

- in the first set (Fig. 6-a -b) the reduced scattering coefficient is constant and equal to 10 cm^{-1}, while the absorption coefficient linearly increases from 0 to 0.49 cm^{-1} at 0.07 cm^{-1} steps (nominal values at 660 nm);
- in the second set (Fig. 6-c -d) the absorption coefficient is constant and equal to 0.07 cm^{-1} at 660 nm, while the reduced scattering coefficient linearly varies from 5 to 20 cm^{-1} at 5 cm^{-1} discrete steps.

The measurement was performed using SiPM 1 and TDC Unit 1 at 40 MHz repetition rate and optical attenuation was used to have a detector count-rate equal to 2 Mcps for every wavelength. The measurement integration time is equal to 1 s and 20 repetitions were acquired. As regards data analysis, firstly a background subtraction was performed and then we applied a non-linear optimal fit to retrieve the two coefficients, based on an analytical model which describes the propagation of photons in a homogeneous diffusive medium [30]. The instrument exhibits good linearity performance in estimating reduced scattering and absorption coefficients with respect to state-of-the-art systems [31].

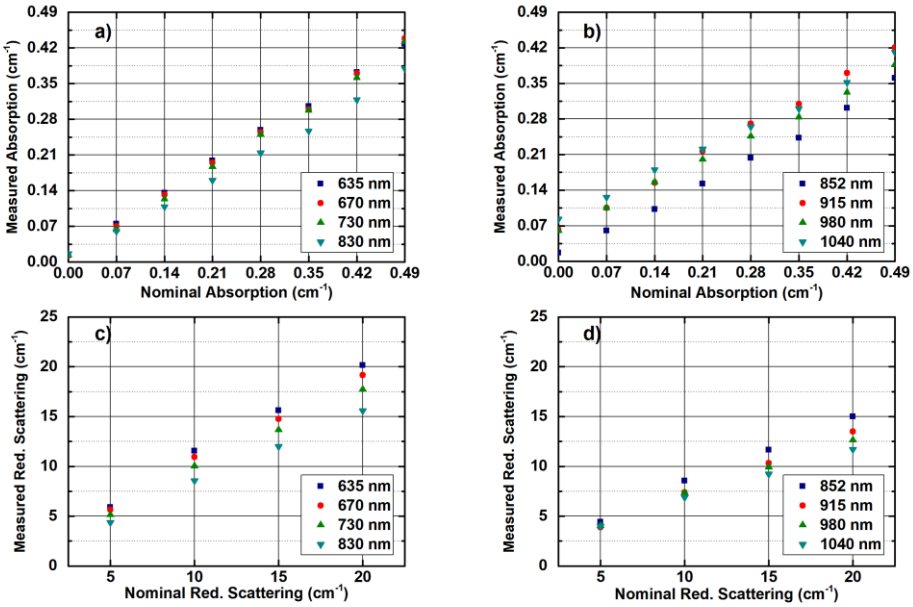

Fig. 6 Linearity of measured absorption and reduced scattering coefficients of solid phantoms. Figures a) and b) show the measured absorption coefficients, while figures c) and d) the measured reduced scattering coefficients. On the left column we report data acquired with the four shortest wavelengths of the instrument (a and c) while longest ones are reported on right column (b and d). Symbols represent average results over 20 repetitions and completely cover error bars, which result lower than 1% of the corresponding value. Nominal absorption and reduced scattering coefficients are quoted at 660 nm.

4. CONCLUSIONS

In this paper, we presented an innovative and full-custom instrument for TR NIRS featuring eight pulsed diode lasers emitting in the near-infrared range and two independent TCSPC channels based on a wide-area SiPM in single-photon counting mode and a fully-custom TDC ASIC fabricated in a 0.35 μm HV CMOS technology. The instrument proved a temporal width of the optical pulses narrower than 135 ps (FWHM) at all the wavelengths, an average output optical power higher than 1 mW at 40 MHz pulse repetition rate and a maximum conversion rate higher than 4 Mconv/s. The instrument provides 10 ps timing resolution and 80 ns measurement range, still guaranteeing a single-shot precision equal to 40 ps (FWHM) and a DNL lower than 1.2% of LSB. Thanks to the FPGA-based architecture, fully-reconfigurable GPIOs and wide-bandwidth connections, the instrument allows to adjust all the measurement parameters in order to perfectly fit applications where a complete TCSPC system is needed.

ACKNOWLEDGMENT

This project is an initiative of the Photonics Public Private Partnership (www.photonics21.org). This work was supported in part by the European Union's Horizon 2020 research and innovation programme under Grant agreement 688303, and in part by the European Commission under H2020 framework with the BITMAP project 675332.

REFERENCES

[1] Johansson J., et al., "Time-Resolved NIR/Vis Spectroscopy for Analysis of Solids: Pharmaceutical Tablets," Appl. Spectr. 56: 725-731, 2002.
[2] Pifferi A., Contini D., Dalla Mora A., Farina A., Spinelli L. and Torricelli A., "New frontiers in time-domain diffuse optics, a review," Journal of Biomedical Optics, vol. 21, no. 9, art. no. 091310, 2016. ISSN: 1083-3668. eISSN: 1560-2281.
[3] Strangman G., Boas D. A. and Sutton J. P., "Non-Invasive Neuroimaging using Near-Infrared Light," Biol. Psychiatry 52: 679-693, 2002.
[4] Gibson A. P. and Dehghani H., "Diffuse optical imaging," Philos.Trans. A: Math. Phys. Eng. Sci. 367(1900), 3055–3072, 2009.
[5] Durduran T., Choe R., Baker W. B. and Yodh A. G., "Diffuse optics for tissue monitoring and tomography," Reports Prog. Phys., vol. 73, no. 7, p. 76701, Jul. 2010.
[6] Vo-Dhin T., "Biomedical photonics handbook," CRC Press, New York, 2003.
[7] Contini D. et al., "Review: Brain and muscle near infrared spectroscopy/imaging techniques," J. Near Infrared Spectrosc., vol. 20, no. 1, pp. 15–27, 2012.
[8] Gibson A.P., Hebden J.C. and Arridge S.R., "Recent advances in diffuse optical imaging," Phys. Med. Biol. 50: 1-43, 2005.
[9] Dalla Mora A., Contini D., Arridge S., Martelli F., Tosi A., Boso G., Farina A., Durduran T., Martinenghi E., Torricelli A. and Pifferi A., "Towards next-generation time-domain diffuse optics for extreme depth penetration and sensitivity," Biomedical Optics Express, vol. 6, no. 5, pp. 1749-1760, 20 April 2015.
[10] Martelli F., Binzoni T., Pifferi A., Spinelli L., Farina A., and Torricelli A., "There's plenty of light at the bottom: statistics of photon penetration depth in random media," Sci. Rep., vol. 6, no. 1, p. 27057, Jul. 2016.
[11] Zucchelli L., Contini D., Re R., Torricelli A., and Spinelli L., "Method for the discrimination of superficial and deep absorption variations by time domain fNIRS," Biomed. Opt. Exp., vol. 4, no. 12, pp. 2893–2910, 2013.
[12] Del Bianco S., Martelli F., and Zaccanti G., "Penetration depth of light re-emitted by a diffusive medium: Theoretical and experimental investigation," Phys. Med. Biol., vol. 47, no. 23, pp. 4131–4144, 2002.
[13] Steinbrink J., Wabnitz H., Obrig H., Villringer A., and Rinneberg H., "Determining changes in NIR absorption using a layered model of the human head," Phys. Med. Biol., vol. 46, no. 3, pp. 879–896, 2001.
[14] Puszka A., Di Sieno L., Dalla Mora A., Pifferi A., Contini D., Planat-Chrétien A., Koenig A., Boso G., Tosi A., Hervé L. and Dinten J.M., "Spatial resolution in depth for time-resolved diffuse optical tomography using short source-detector separations," Biomedical Optics Express, vol. 6, no. 1, pp. 1 - 10, 1 January 2015.

[15] Markovic B., Tisa S., Villa F. A., Tosi A., and Zappa F., "A high-linearity, 17 ps precision time-to-digital converter based on a single-stage Vernier delay loop fine interpolation," IEEE Trans. Circuits Syst. I, Reg. Papers, vol. 60, no. 3, pp. 557–569, Mar. 2013.
[16] Behera A., Di Sieno L., Pifferi A., Martelli F., Dalla Mora A., "Instrumental, optical and geometrical parameters affecting time-gated diffuse optical measurements: a systematic study," Biomedical Optics Express, vol. 9, no. 11, pp.5524-5542, 1 November 2018.
[17] Becker & Hickl Gmbh, "BDS-MM Family Picosecond Diode Lasers." [Online]. Available: https://www.becker-hickl.com/pdf/db-bds-mm-family-extd-08.pdf. Accessed Jan. 5, 2019.
[18] Picoquant Gmbh, "LDH Series – Picosecond Pulsed Diode Laser Heads." [Online]. Available: https://www.picoquant.com/products/category/picosecond-pulsed-sources/ldh-series-picosecond-pulsed-diode-laser-heads. Accessed Jan. 5, 2019.
[19] Buttafava M. et al., "A Compact Two-Wavelength Time-Domain NIRS System Based on SiPM and Pulsed Diode Lasers," in IEEE Photonics Journal, vol. 9, no. 1, pp. 1-14, Feb. 2017.
[20] Paulus P., Langenhorst R. and Jager D., "Generation and optimum control of picosecond optical pulses from gain-switched semiconductor lasers," in IEEE Journal of Quantum Electronics, vol. 24, no. 8, pp. 1519-1523, Aug. 1988.
[21] Renna M. et al., "Compact dual-wavelength system for time-resolved diffuse optical spectroscopy," 2017 13th Conference on Ph.D. Research in Microelectronics and Electronics (PRIME), Giardini Naxos, 2017, pp. 293-296.
[22] Hamamatsu Photonics K.K., "Photomultiplier Tube Handbook", 2007.
[23] Gulinatti A., Maccagnani P., Rech I., Ghioni M. and Cova S., "35 ps time resolution at room temperature with large area single photon avalanche diodes," in IET Electronics Letters, vol. 41, no. 5, pp. 272-274, March 2005.
[24] Sanzaro M., Gattari P., Villa F. A., Tosi A., Croce G. and Zappa F., "Single-Photon Avalanche Diodes in a 0.16 μm BCD Technology With Sharp Timing Response and Red-Enhanced Sensitivity," in IEEE Journal of Selected Topics in Quantum Electronics, vol. 24, no. 2, pp. 1-9, March-April 2018.
[25] Martinenghi E., Dalla Mora A., Contini D., Farina A., Villa F., Torricelli A., Pifferi A., "Spectrally resolved single-photon timing of silicon photomultipliers for time-domain diffuse optics," Photonics Journal, IEEE, vol. 7, no. 4, pp. 6802512-1 – 6802512-12, August 2015. ISSN: 1943-0655.
[26] Martinenghi E., Di Sieno L., Contini D., Sanzaro M., Pifferi A. and Dalla Mora A., "Time-resolved single-photon detection module based on silicon photomultiplier: A novel building block for time-correlated measurement systems", Review of Scientific Instruments, 87, 073101, 2016.
[27] Picoquant Gmbh, "HydraHarp 400 - Multichannel Picosecond Event Timer & TCSPC Module." [Online]. Available: https://www.picoquant.com/products/category/tcspc-and-time-tagging-modules/hydraharp-400-multichannel-picosecond-event-timer-tcspc-module. Accessed Jan. 6, 2019.
[28] Becker & Hickl Gmbh, "SPC-130 Low cost TCSPC module." [Online]. Available: http://www.becker-hickl.de/pdf/dbspc130-2.pdf. Accessed Jan. 6, 2019.
[29] Pifferi A., Torricelli A., Bassi A., Taroni P., Cubeddu R., Wabnitz H., Grosenick D., Möller M., Macdonald R., Swartling J., Svensson T., Andersson-Engels S., van Veen R. L. P., Sterenborg H. J. C. M., Tualle J.-M., Nghiem H. L., Avrillier S., Whelan M. and Stamm H., "Performance assessment of photon migration instruments: the MEDPHOT protocol," Appl. Opt. 44, 2104–2114 (2005).
[30] Martelli F., Del bianco S., Ismaelli A. and Zaccanti G., [Light Propagation through Biological Tissue and Other Diffusive Media: Theory, Solutions, and Software], SPIE Press, Bellingham, Washington (2009).
[31] Konugolu Venkata Sekar S. et al., "Broadband (600–1350 nm) Time-Resolved Diffuse Optical Spectrometer for Clinical Use," (2016) IEEE Journal of Selected Topics in Quantum Electronics, 22(3), pp. 406-414.